


# Multiparametric MRI Radiomic Model for Preoperative Predicting WHO/ISUP Nuclear Grade of Clear Cell Renal Cell Carcinoma

Qiong Li, MD,<sup>1,2#</sup> Yu-jia Liu, BS,<sup>3,4#</sup> Di Dong, PhD,<sup>3,4#</sup> Xu Bai, MS,<sup>2</sup> Qing-bo Huang, MD,<sup>5</sup> Ai-tao Guo, MD,<sup>6</sup> Hui-yi Ye, MD,<sup>2</sup> Jie Tian, PhD,<sup>4,7\*</sup> and Hai-yi Wang, MD<sup>2\*</sup> 

**Background:** Nuclear grade is of importance for treatment selection and prognosis in patients with clear cell renal cell carcinoma (ccRCC).

**Purpose:** To develop and validate an MRI-based radiomic model for preoperative predicting WHO/ISUP nuclear grade in ccRCC.

**Study Type:** Retrospective.

**Population:** In all, 379 patients with histologically confirmed ccRCC. Training cohort ( $n = 252$ ) and validation cohort ( $n = 127$ ) were randomly assigned.

**Field Strength/Sequence:** Pretreatment 3.0T renal MRI. Imaging sequences were fat-suppressed T<sub>2</sub>WI, contrast-enhanced T<sub>1</sub>WI, and diffusion weighted imaging.

**Assessment:** Three prediction models were developed using selected radiomic features, radiomic and clinicoradiologic characteristics, and a model containing only clinicoradiologic characteristics. Receiver operating characteristic (ROC) curves and area under the curve (AUC) were used to assess the predictive performance of these models in predicting high-grade ccRCC.

**Statistical Tests:** The least absolute shrinkage and selection operator (LASSO) and minimum redundancy maximum relevance (mRMR) method were used for the selection of radiomic features and clinicoradiologic characteristics, respectively. Multivariable logistic regression analysis was used to develop the radiomic signature of radiomic features and clinicoradiologic model of clinicoradiologic characteristics.

**Results:** The radiomic signature showed good performance in discriminating high-grade (grades 3 and 4) from low-grade (grades 1 and 2) ccRCC, with sensitivity, specificity, and AUC of 77.3%, 80.0%, and 0.842, respectively, in the validation cohort. The radiomic model, combining radiomic signature and clinicoradiologic characteristics, displayed good predictive ability for high-grade with sensitivity, specificity, and accuracy of 63.6%, 93.3%, and 88.2%, respectively, in the validation cohort. The radiomic model showed a significantly better performance than the clinicoradiologic model ( $P < 0.05$ ).

View this article online at [wileyonlinelibrary.com](http://wileyonlinelibrary.com). DOI: 10.1002/jmri.27182

Received Mar 3, 2020, Accepted for publication Apr 17, 2020.

\*Address reprint requests to: J.T., CAS Key Laboratory of Molecular Imaging, Institute of Automation, Chinese Academy of Sciences, No. 95, Zhongguancun East Road, Haidian District, Beijing 100191, China. E-mail: [jie.tian@ia.ac.cn](mailto:jie.tian@ia.ac.cn) or H.-y.W., Department of Radiology, First Medical Center, Chinese PLA General Hospital, No. 28, Fuxing Road, Haidian District, Beijing 100853, China. E-mail: [wanghaiyi301@outlook.com](mailto:wanghaiyi301@outlook.com)

<sup>#</sup>These authors contributed equally to this work.

Contract grant sponsor: National Natural Science Foundation of China; Contract grant numbers: 81971580, 91959130, 81971776, 81771924, 81930053; Contract grant sponsor: National Key R&D Program of China; Contract grant numbers: 2017YFA0205200, 2017YFC1308700, 2017YFC1309100; Contract grant sponsor: Beijing Natural Science Foundation; Contract grant number: L182061; Contract grant sponsor: Medical Big Data Research and Development Project of Chinese PLA General Hospital; Contract grant number: 2018MBD-023; Contract grant sponsor: Youth Innovation Promotion Association CAS; Contract grant number: 2017175.

From the <sup>1</sup>Department of Radiology, Tianjin Nankai Hospital (Tianjin Hospital of Integrated Traditional Chinese and Western Medicine), Tianjin, China;

<sup>2</sup>Department of Radiology, First Medical Center, Chinese PLA General Hospital, Beijing, China; <sup>3</sup>School of Artificial Intelligence, University of Chinese Academy of Sciences, Beijing, China; <sup>4</sup>CAS Key Laboratory of Molecular Imaging, Institute of Automation, Chinese Academy of Sciences, Beijing, China;

<sup>5</sup>Department of Urology, First Medical Center, Chinese PLA General Hospital, Beijing, China; <sup>6</sup>Department of Pathology, First Medical Center, Chinese PLA General Hospital, Beijing, China; and <sup>7</sup>Beijing Advanced Innovation Center for Big Data-Based Precision Medicine, School of Medicine, Beihang University, Beijing, China

Additional supporting information may be found in the online version of this article

**Data Conclusion:** Multiparametric MRI-based radiomic model can predict WHO/ISUP grade in patients with ccRCC with satisfying performance, and thus could help the physician to improve treatment decisions.

**Level of Evidence:** 3

**Technical Efficacy Stage:** 2

J. MAGN. RESON. IMAGING 2020.

**C**LEAR CELL RENAL CELL CARCINOMA (ccRCC) is the most common subtype of renal cell carcinoma and accounts for ~90% of kidney tumors.<sup>1</sup> The major risk factors of renal cell carcinoma include smoking, obesity, and hypertension.<sup>1,2</sup> Tumor nuclear grade is one of the well-known prognostic factors of ccRCC and considered as an independent predictor of cancer-specific survival.<sup>1,3</sup> In 2016, the WHO classification of tumors of the kidney, the WHO/ISUP system, was recommended for ccRCC grading.<sup>4</sup> Radical operations are acceptable for high-grade ccRCC, while minimally invasive techniques are more feasible management considerations for low-grade ccRCC, such as nephron-sparing surgery, ablation, and even active surveillance.<sup>2</sup> In order to evaluate the malignant degree of tumor and make an optimal treatment plan, preoperative pathological stratification is important. Percutaneous biopsy is of great help in confirming the grade of ccRCC; however, it is associated with a risk of procedural complications, potential sampling errors, failure to perform nuclear grading, and mismatch with pathology outcome.<sup>5</sup>

Renal magnetic resonance imaging (MRI), a crucial tool for preoperative diagnosis in ccRCC, facilitates noninvasive assessment. Previous studies have found that some MRI features contributed to preoperative grading of ccRCC, including tumor size, hemorrhage, necrosis, enhancement degree, and vein thrombosis.<sup>6–9</sup>

Radiomics is an emerging and promising technique and has been widely applied in the field of oncology. It converts medical images into high dimensional and quantitative image features by means of computer postprocessing technology. By utilizing model-building algorithms, radiomic features can show associations with tumor histopathology and heterogeneity.<sup>10–14</sup> Several studies have indicated that the increasing heterogeneity on MRI reflected by radiomics was associated with the histological grade of cervical cancer and prostate cancer.<sup>15,16</sup>

The purpose of this study was to develop and validate an MRI-based radiomic model for preoperative prediction of ccRCC WHO/ISUP nuclear grade.

## Materials and Methods

### Patients

Ethical approval was obtained from the Institutional Review Board of our institute for this retrospective study and the requirement for informed consent was waived.

Patients with pathologically proven ccRCC from January 2016 to November 2017, with preoperative multiparametric renal

MRI on GE (Milwaukee, WI) 3.0T scanners, were included. The initial query yielded a target population of 425 patients who were considered eligible for inclusion in the study. Exclusive criteria included: 1) patients who received previous treatment or experienced postoperative recurrence of ccRCC; 2) MRI images with remarkable artifact (determined by three radiologists: Q.L., X.B., H.Y.Y.); 3) WHO/ISUP nuclear grade was not available; 4) the diameter of the mass in an axial plane less than 1 cm; or 5) the time interval between MRI examination and following surgical resection was more than 1 month.

The flowchart of the study population recruitment is shown in Fig. 1. Finally, our study enrolled 379 patients (age range, 24–87 years old): 88 (23%) female and 291 (77%) male, with a median age of 54 years. In this study the tumor size ranged from 1.23–14.87 cm. Of all tumors, 206 lesions were less than 4 cm, 119 lesions were between 4 cm and 7 cm, and 54 lesions were more than 7 cm. The entire dataset was randomly assigned to a training cohort ( $n = 252$ ) and a validation cohort ( $n = 127$ ) at a ratio of 2:1.

### MRI Acquisition

MR sequences included axial fat-suppressed T<sub>2</sub>WI (weighted images), diffusion-weighted imaging (DWI) (apparent diffusion coefficient [ADC] calculation thereafter), and dynamic contrast-enhanced scans. The details of the MRI equipment and MRI scan protocol are shown in Supplementary A1 and Table S1.

### Histopathological Assessment of Nuclear Grade

WHO/ISUP nuclear grade was recorded from pathology reports of histopathological examination in our institute. The specimens were from the biopsy of one patient, radical nephrectomy of 127 patients, and partial nephrectomy of 251 patients. A dedicated genitourinary pathologist (A.T.G.) rechecked the WHO/ISUP nuclear grade of all the slides. These tumors were divided into low-grade (grades 1 and 2) and high-grade (grades 3 and 4).

### Clinicoradiologic Model Building

The clinicoradiologic characteristics were collected from clinical risk factors, tumor size, and subjective MRI scores. Clinical risk factors included gender, age at diagnosis, body mass index (BMI), smoking (former or current smoker) or not, and hypertension (previous or current diagnosis of hypertension) or not. The tumor size was the maximal diameter measured on the axial fat-suppressed T<sub>2</sub>WI image. The criteria for the subjective MRI scores is shown in Supplementary A2 and Table S2.

Univariate analysis was performed to assess the potential association between clinicoradiologic characteristics and nuclear grade. The normality of all data was analyzed using the Shapiro–Wilk method. Differences in clinicoradiologic characteristics between low- and high-grade were assessed using the independent Student's *t*-test

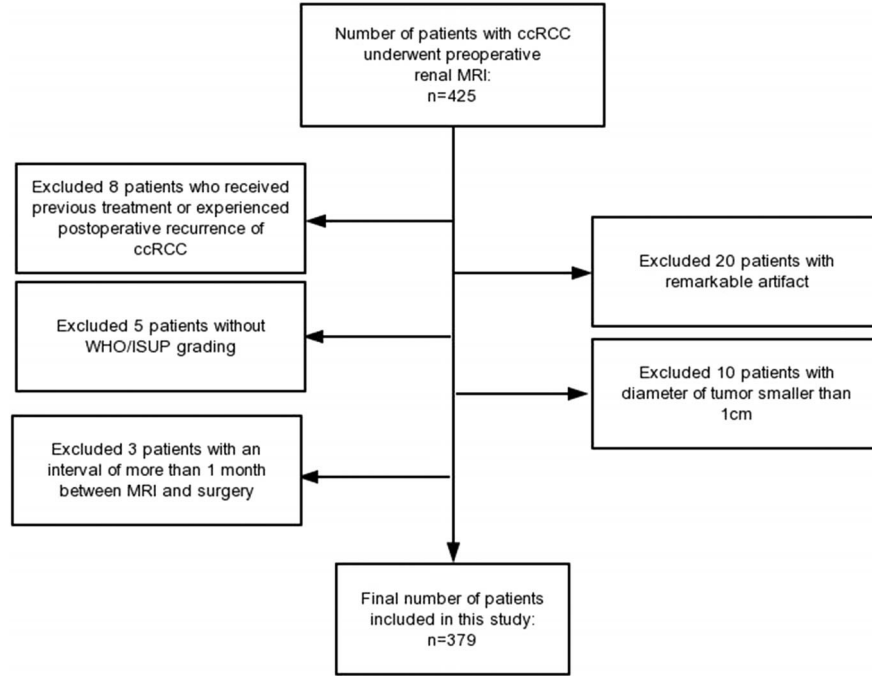


FIGURE 1: Flowchart of study population recruitment.

or Mann–Whitney  $U$ -test for continuous variables, and Fisher’s exact test or  $\chi^2$  test for categorical variables.

The minimum redundancy maximum relevance (mRMR) method<sup>17</sup> was carried out for ranking the clinicoradiologic characteristics with mutual information. The clinicoradiologic model was built using multivariable logistic regression on clinical characteristics in the training cohort.

### MRI Radiomic Signature Building

**TUMOR SEGMENTATION AND RADIOMIC FEATURE EXTRACTION.** All MR images were exported from the picture archiving and communication systems (PACS) and then transferred to an independent workstation for manual segmentation using ITK-SNAP 3.6 software (www.itk-snap.org). For each tumor, an

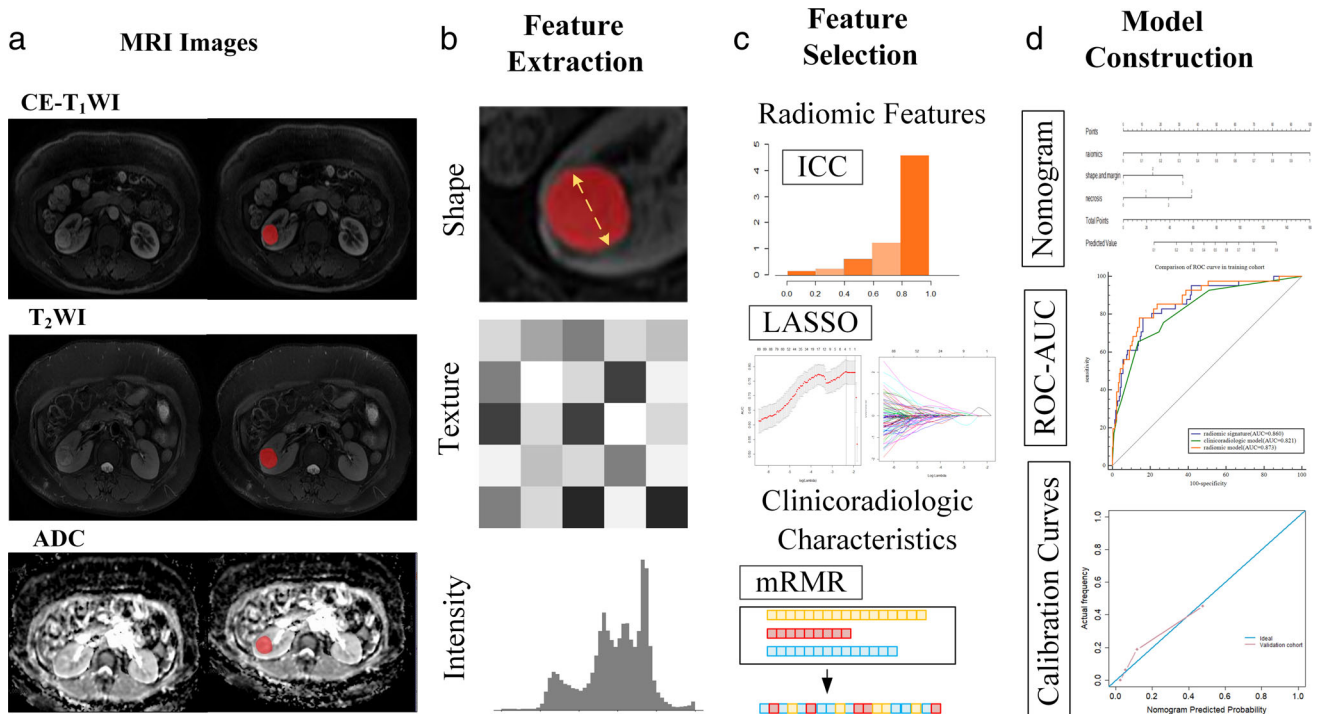


FIGURE 2: Radiomic workflow in this study. (a) Tumor segmentation by radiologists. (b) Feature extraction from tumor region. (c) Feature selection by ICC and LASSO method and clinicoradiologic characteristics by mRMR. (d) Model construction and validation.

abdominal radiologist (Q.L., with 10-year experience in abdominal MRI diagnosis) drew a free-hand 3D region of interest (ROI) on each slice of the axial fat-suppressed T<sub>2</sub>WI, ADC map, and corticomedullary phase of contrast-enhanced T<sub>1</sub>WI (CE-T<sub>1</sub>WI). As shown in Fig. 2, the ROI was drawn along the contour of the lesion, and the top and bottom layers of the lesion were abandoned to avoid the partial volume effect.

A total of 4224 radiomic features of the three sequences (1408 features per sequence) were extracted from the ROIs, included in four groups: 1) image intensity (first-order features); 2) shape and size-based features; 3) textural features; and 4) wavelet features.<sup>18</sup> All features extraction methods were implemented using the Pyradiomics package (<https://pyradiomics.readthedocs.io/en/latest/>) based on Python (v. 3.6.5, <https://www.python.org/>).

**INTER- AND INTRAOBSERVER RADIOMIC FEATURE EXTRACTION REPRODUCIBILITY.** Fifty patients were randomly selected for intraobserver and interobserver reproducibility test. The radiologist (Q.L.) and another abdominal radiologist (X.B., with 5-year experience in abdominal MRI diagnosis) outlined the ROI again 30 days after the initial segmentation. The intraclass correlation coefficient (ICC) was used to assess the agreement of extracted features by intraobserver and interobserver segmentations. An ICC greater than 0.75 was considered in great agreement and highly robust.<sup>19</sup>

**RADIOMIC FEATURE SELECTION AND RADIOMIC SIGNATURE BUILDING.** Radiomic signature building was performed in the training cohort. The feature selection and signature building processes were separately performed on each sequence. The steps were as follows: first, filtering out the features with ICCs  $\leq 0.75$  in the intraobserver or interobserver test; second, refining the most useful prognostic features using the least absolute shrinkage and selection operator (LASSO) method; finally, using logistic regression of the selected features weighted by their coefficients to build a signature. After those steps, three signatures of three sequences (fat-suppressed T<sub>2</sub>WI, CE-T<sub>1</sub>WI, and ADC) were separately built. Then a radiomic signature was generated via the linear combination of the three signatures.

**COMBINED MODEL, MODEL VALIDATION, AND NOMOGRAM CONSTRUCTION.** Multivariable logistic regression analysis was used to develop a combined radiomic model using radiomic signature and clinicoradiologic characteristics. Model performance was validated in terms of the receiver operating characteristic (ROC) curve and area under the curve (AUC). Sensitivity, specificity, positive predictive value (PPV), negative predictive value (NPV), and accuracy were also calculated. The Delong test was used to explore whether the radiomic model performed better than the clinicoradiologic model and radiomic signature. Additionally, the nomogram of the best model was established for visible use. The calibration curves were applied to modify and reduce the bias of the final model. Also, stratified analysis was applied on a different MR scanner in the three models to figure out the difference between scanners in predicting efficiency.

**TABLE 1. Clinical Characteristics of Patients in the Training and Validation Cohorts**

Characteristic	Training cohort			Validation cohort		
	low-grade	high-grade	P	low-grade	high-grade	P
Number	211	41	/	105	22	/
Age (years)	53 $\pm$ 11	59 $\pm$ 11	<0.05	55 $\pm$ 12	59 $\pm$ 11	0.138
Gender	161 M, 50 W	31 M, 10 W	0.924	81 M, 24 W	18 M, 4 W	0.631
BMI	25.59 $\pm$ 3.21	25.15 $\pm$ 3.26	0.422	26.22 $\pm$ 3.68	25.09 $\pm$ 4.21	0.251
History of smoking	94/211	14/41	0.218	39/105	12/22	0.130
Hypertension	78/211	21/41	0.087	44/105	10/22	0.759
Tumor size	4.04 $\pm$ 2.16	6.03 $\pm$ 2.84	<0.05	4.22 $\pm$ 2.40	6.64 $\pm$ 3.42	<0.05

BMI = body mass index; M = men; W = women.

### Statistical Analysis

The statistical analyses were performed with R software (v. 3.5.3; R Foundation for Statistical Computing, Vienna, Austria) and Python software (v. 3.6.0). The tests were two-sided and  $P < 0.05$  was considered statistically significant.

## Results

### Clinical Characteristics

The clinical characteristics of patients in the training and validation cohorts are shown in Table 1. The training cohort included 252 patients (192 male and 60 female; median age, 54 years; age range, 27–86 years), and 127 patients were included in the validation cohort (99 male and 28 female; median age, 55 years; age range, 24–87 years). Except for age ( $P < 0.05$ ) and tumor size ( $P < 0.05$ ), there was no significant difference in gender ( $P = 0.924$ ), BMI ( $P = 0.422$ ), history of smoking ( $P = 0.218$ ), and hypertension ( $P = 0.087$ ) between the two groups in the training cohort. In the validation cohort, except for tumor size ( $P < 0.05$ ), no differences were found between the two groups in terms of age ( $P = 0.138$ ), gender ( $P = 0.631$ ), BMI ( $P = 0.251$ ), history of smoking ( $P = 0.130$ ), and hypertension ( $P = 0.759$ ).

### Predictive Performance of the Clinicoradiologic Model

There were significant differences between low-grade and high-grade ccRCC in the training cohort with age, tumor size, subjective MRI score of pseudocapsule, shape and margin, hemorrhage, hypervascularity, intratumoral neovascularity, peritumoral neovascularity, cystic-solid, vein thrombosis, lymphadenopathy, necrosis, and perinephric invasion (Table S3).

The mRMR selected the top five clinicoradiologic characteristics correlated with nuclear grade, including shape and margin, vein thrombosis, lymphadenopathy, necrosis, and perinephric invasion. In multivariable logistic regression analysis, only shape and margin and necrosis were independent

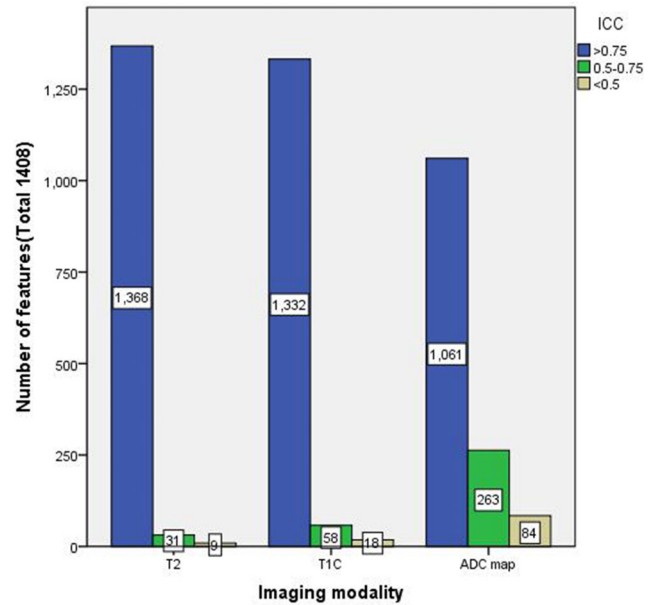


FIGURE 3: Intraclass correlation coefficient (ICC) analysis.

factors of high-grade ccRCC, and thus they were used to build the clinicoradiologic model (Table 2).

The clinicoradiologic model showed good performance of ccRCC grading, which reached an AUC of 0.821 (95% confidence interval [CI], 0.768–0.867) in the training cohort, and AUC of 0.777 (95% CI, 0.695–0.846) in the validation cohort.

### Radiomic Feature Selection and Radiomic Model Building

According to the standard of the ICC >0.75 in the intraobserver and interobserver tests, 1368 radiomic features from T<sub>2</sub>WI images, 1332 features from CE-T<sub>1</sub>WI images, and 1061 features from the ADC map were highly robust and selected for further analysis (Fig. 3). LASSO and logistic regression revealed two features from T<sub>2</sub>WI to construct the T<sub>2</sub>WI signature, three key features from CE-T<sub>1</sub>WI to build the CE-T<sub>1</sub>WI signature, and seven features from ADC images to build the ADC signature. The AUCs of the T<sub>2</sub>WI,

TABLE 2. Multivariate Logistic Regression Analysis of the Clinicoradiologic Model

	$\beta$	OR	95% CI	$p$
Intercept	4.253			
Shape and margin	−1.192	0.304	0.145–0.635	<0.05
Vein thrombosis	−0.593	0.553	0.196–1.558	0.262
Lymphadenopathy	−0.864	0.421	0.137–1.298	0.132
Necrosis	−0.755	0.470	0.286–0.772	<0.05
Perinephric invasion	−0.402	0.669	0.231–1.936	0.459

CI = confidence interval; OR = odds ratio.

**TABLE 3. Radiomic Features Selection From the MRI in the Training Cohort**

	Feature selected	Group	P-value
T <sub>2</sub> WI	“exponential_gldm_LargeDependenceEmphasis”	texture	<0.05
	“square_glrlm_RunPercentage”	texture	<0.05
CE-T <sub>1</sub> WI	“original_shape_Sphericity”	shape	<0.05
	“wavelet.HLL_glcmlm2”	texture	<0.05
	“lbp.2D_glszm_SizeZoneNonUniformity”	texture	<0.05
ADC	“original_firstorder_Mean”	intensity	<0.05
	“original_firstorder_Median”	intensity	<0.05
	“wavelet.HLL_glszm_LargeAreaLowGrayLevelEmphasis”	texture	<0.05
	“exponential_glcmlm2”	texture	<0.05
	“exponential_glrlm_ShortRunLowGrayLevelEmphasis”	texture	<0.05
	“exponential_ngtdm_Busyness”	texture	<0.05
	“square_firstorder_Median”	intensity	<0.05

ADC = apparent diffusion coefficient; CE-T<sub>1</sub>WI = contrast-enhanced T<sub>1</sub>WI; MRI = magnetic resonance imaging. The description of the radiomic features mentioned above is displayed in the Supplementary A3.

CE-T<sub>1</sub>WI, and ADC signatures were 0.794 (95% CI, 0.761–0.926), 0.804 (95% CI, 0.636–0.861), and 0.850 (95% CI, 0.639–0.864), respectively, in the training cohort. The three signatures were chosen for radiomic signature construction (Table 3).

The AUC of the radiomic signature was 0.860 (95% CI, 0.811–0.900) in the training cohort and 0.842 (95% CI, 0.767–0.901) in the validation cohort.

### Construction of a Combined Radiomic Model and Nomogram

The combined radiomic model of radiomic signature and clinicoradiologic characteristics showed a prediction performance

of high-grade ccRCC, which reached an AUC of 0.873 (95% CI, 0.826–0.912) in the training cohort, and an AUC of 0.845 (95% CI, 0.770–0.903) in the validation cohort. The ROC curves of the radiomic signature, clinicoradiologic model, and radiomic model in the training and validation cohorts are shown in Fig. 4.

The performance of all models in the validation cohort is shown in Table 4. The AUC of the radiomic model was significantly better than that of the clinicoradiologic model ( $Z = 2.960$ ,  $P < 0.05$ ). However, there was no significant difference of AUC between the radiomic model and the radiomic signature ( $Z = 0.184$ ,  $P = 0.854$ ), or between the radiomic signature and clinicoradiologic model ( $Z = 1.740$ ,

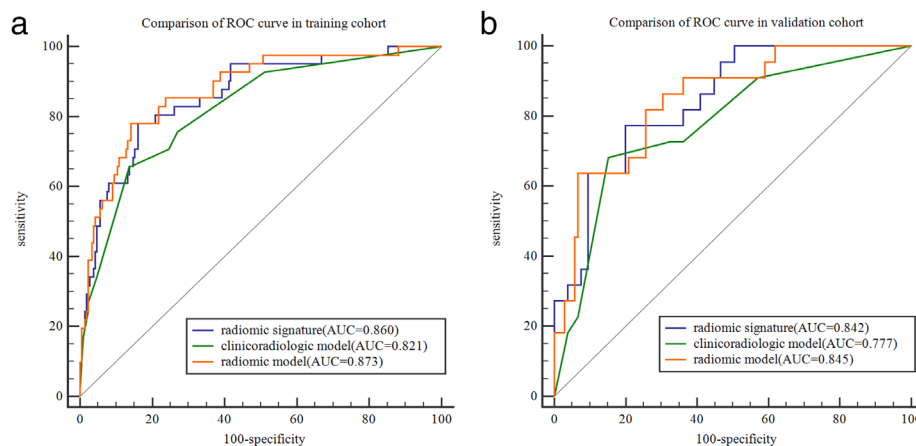


**FIGURE 4:** Comparison of the AUC of radiomic signature, clinicoradiologic model, and radiomic model in the training and validation cohorts. (a) ROC curves of three models in training cohort. (b) ROC curves of three models in the validation cohort.



**TABLE 4. Predictive Performance of the Three Models for Preoperative ccRCC Grading in the Validation Cohort**

Model	AUC [95% CI]	Sensitivity (%)	Specificity (%)	PPV (%)	NPV (%)	Accuracy (%)
Clinicoradiologic model	0.777 [0.695–0.846]	68.2 (15/22)	84.8 (89/105)	48.4 (15/31)	92.7 (89/96)	81.9 (104/127)
Radiomic signature	0.842 [0.767–0.901]	77.3 (17/22)	80.0 (84/105)	44.7 (17/38)	94.4 (84/89)	79.5 (101/127)
Radiomic model	0.845 [0.770–0.903]	63.6 (14/22)	93.3 (98/105)	66.7 (14/21)	92.5 (98/106)	88.2 (112/127)

AUC = area under the curve; ccRCC = clear cell renal cell carcinoma; CI = confidence interval; NPV = negative predictive value; PPV = positive predictive value.

$P = 0.082$ ). Compared with the other two models, the radiomic model yielded the highest specificity and accuracy.

The nomogram of radiomic model is illustrated in Fig. 5a, which could facilitate nuclear grading in clinical practice (Fig. 6). Figure 5b,c demonstrates the calibration curves of the radiomic model, which indicated that there was a good calibration of the prediction result of the radiomic model and the real result. The stratified analysis demonstrated that there was no obvious difference in predicting high-grade ccRCC between the two scanners (Supplementary A4 and Fig. S1).

## Discussion

In this retrospective study we developed and validated a multiparametric MRI-based radiomic model for noninvasively predicting high-grade ccRCC.

With recent advances in imaging technique and post-processing analysis, MRI can serve as a diagnostic, therapeutic, and prognostic biomarker for renal cell carcinoma.<sup>20</sup> However, the MRI findings of low-grade and high-grade ccRCC overlap in some cases. Moreover, previous studies are not completely consistent on which MRI features are valuable

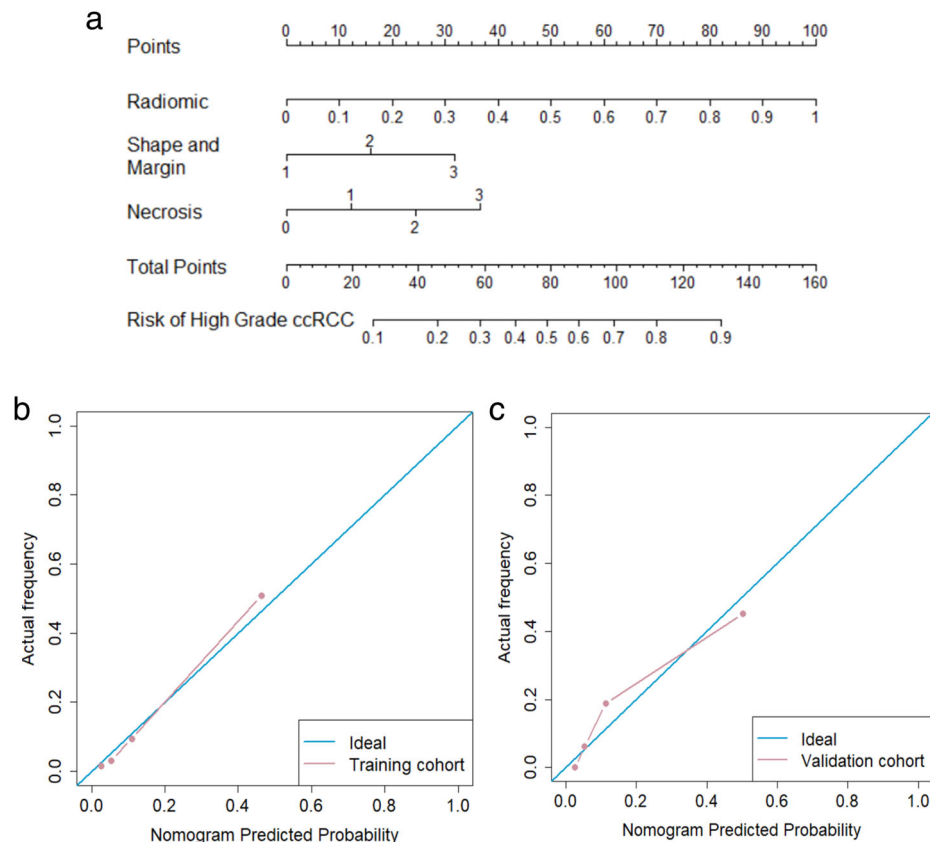


**FIGURE 5: Radiomic nomogram and its calibration curves. (a) Nomogram of radiomic model for prediction of high-grade in patients with ccRCC. (b) Calibration curve of the nomogram in the training cohort. (c) Calibration curve of the nomogram in the validation cohort.**

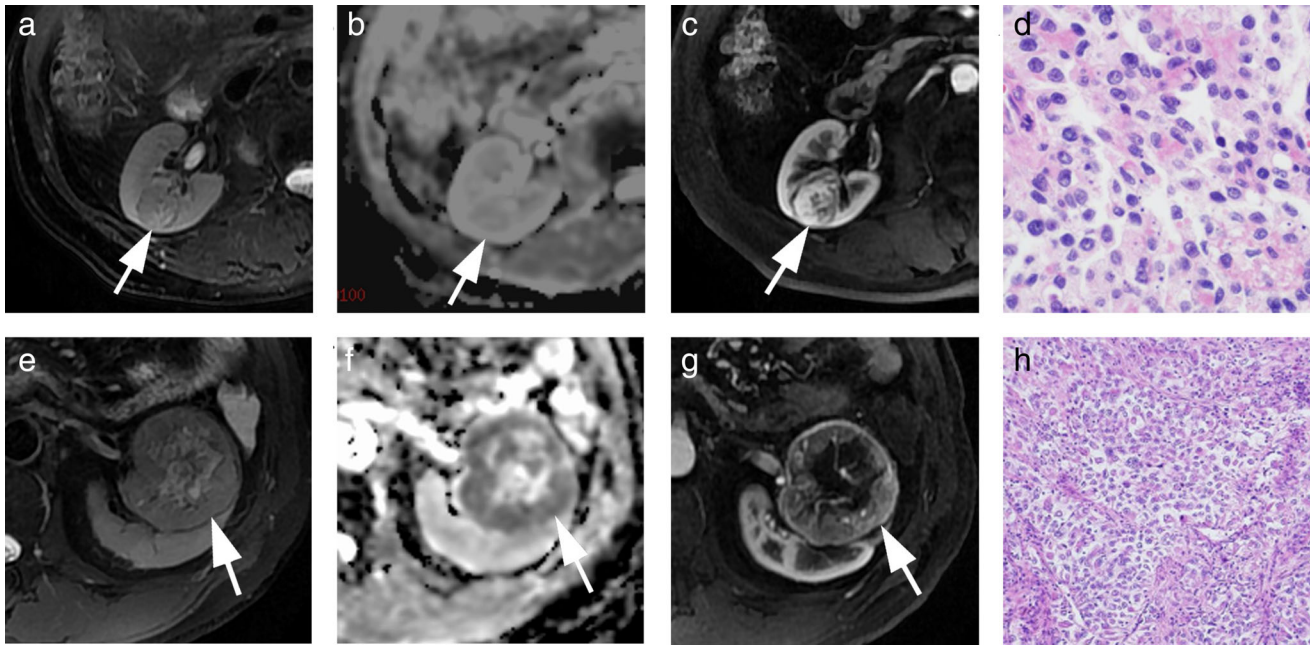


**FIGURE 6:** Two cases with ccRCC. **a–d:** Preoperative MRI in a 73-year-old man with ccRCC of WHO/ISUP grade 2 in the right kidney. Considering the radiomic signature of 0.049, shape and margin of 1, and necrosis of 0, the risk of high-grade ccRCC was smaller than 0.1 according to the nomogram. (a) Axial fat-suppressed T<sub>2</sub>WI showed a round-shaped, well-defined, solid mass. (b) The lesion showed similar signal compared with renal parenchyma on the ADC map. (c) On corticomedullary phase of contrast-enhanced T<sub>1</sub>WI, the lesion showed significant enhancement. (d) The tumor cells were relatively small, with clear cytoplasm, small to moderate nucleus with round shape, small nucleolus (hematoxylin–eosin staining, 40× magnification). **e–h:** Preoperative MRI in a 52-year-old man with ccRCC of WHO/ISUP grade 3 in the left kidney. Considering the radiomic signature of 0.586, shape and margin of 1, and necrosis of 2, the risk of high-grade ccRCC was 0.6 according to the nomogram. (e) Axial fat-suppressed T<sub>2</sub>WI showed a round-shaped, well-defined, solid mass with central necrosis. (f) The lesion showed lower signal than renal parenchyma on the ADC map. (g) Compared with the renal cortex, the lesion showed slight enhancement with intratumoral vessel on corticomedullary phase of contrast-enhanced T<sub>1</sub>WI. (h) The tumor cells were large, with clear or eosinophilic cytoplasm and obvious nucleolus (hematoxylin–eosin staining, 10× magnification).

for nuclear grading.<sup>6,8</sup> Therefore, it is challenging to use morphological evaluation of MRI for nuclear grading in ccRCC. Fortunately, radiomics can reveal the subtle differences of the intensity distribution in medical images, which cannot be easily recognized by human eyes, with the pattern of signal distribution reflecting the heterogeneity of tumors.<sup>21</sup> Previous studies have investigated the potential of computed tomography (CT)-based radiomic to predict Fuhrman nuclear grade of ccRCC.<sup>22,23</sup> However, there are some limitations to using CT. First, the Fuhrman grading system has poor interobserver reproducibility.<sup>24</sup> Second, in contrast to CT, MRI provides multiple forms of soft-tissue contrast, as well as functional parameters and permits a comprehensive evaluation of ccRCC.<sup>25</sup> Recently, a study using MRI and radiomics to predict nuclear grade in ccRCC patients demonstrated that the predictive accuracy of their radiomic signature (74%) was lower than ours (88.2%).<sup>26</sup> We think that the ADC data and wavelet analysis used in our method improve predictive accuracy.

In this study the clinoradiologic model performed well in predicting high-grade ccRCC. In multivariate analysis of clinical risk factors and subjective MRI scores, only shape and margin and necrosis were independent predictors of high-grade ccRCC. The margin of low-grade ccRCC lesions was

regular, and a round shape was often observed. The high-grade ccRCC lesions tend to be aggressive, with an irregular shape and ill-defined margin, with the presence of necrosis and perinephric fat invasion or distant metastasis. Necrosis has been demonstrated to be an independent predictor of high-grade ccRCC in previous studies.<sup>6,8</sup> Coy et al reported that high-grade ccRCC lesions showed ill-defined tumor margins.<sup>27</sup> Wei et al showed that the tumor shape differed significantly between low-grade and high-grade ccRCC.<sup>28</sup> Two MRI characteristics (shape and margin, necrosis) extracted in this study were consistent with previous studies,<sup>8,27,28</sup> reflecting the features of invasive growth and uneven distribution of blood supply in high-grade ccRCC.

By revealing the heterogeneity of tumors, the radiomic signature has been more and more used to predict the degree of malignancy. In our study, the radiomic signature from MRI showed excellent performance in predicting high-grade ccRCC. The 12 radiomic features in the final radiomic signature included two features from T<sub>2</sub>WI, three features from CE-T<sub>1</sub>WI, and seven features from the ADC map. Most of these radiomic features were obtained from exponential or wavelet filtered images, which were high-dimensional features and could not be easily deciphered by humans. The results suggest that



combining multiple MRI sequences allowed the collection of more valuable information of the tumor than a single sequence. T<sub>2</sub>WI could provide morphological features of ccRCC, including pseudocapsule, cystic components, and necrosis, which are often seen in high-grade ccRCC.<sup>6</sup> ccRCC commonly exhibits hypervascularity, and CE-T<sub>1</sub>WI can show the enhancement degree and neovascularization within the tumor.<sup>29</sup> DWI could provide excellent tissue contrast based on the molecular diffusion of water within tumors, and the reported ADC has been associated with the degree of malignancy in tumors.<sup>8</sup>

The radiomic model combined with radiomic signature and clinicoradiologic characteristics significantly improved the predictive performance in contrast to the clinicoradiologic model. A meta-analysis of the percutaneous biopsy revealed that the median concordance rate between grading on biopsy and the surgical specimen was 87% using the two-tier (high vs. low) grading system,<sup>30</sup> while our radiomic model achieved a similar diagnostic accuracy of 88.2% with noninvasive preoperative MRI. Therefore, the radiomic model may eventually be a supplement to percutaneous biopsy.

### Limitations

The present study had several limitations. First, our model was trained and validated using retrospective data obtained from a single institution, which could yield an unintentional selection bias. A large-scale prospective and multicenter study is needed to validate our results. Second, in this study the diameter of lesions in many cases was more than 4 cm. Future studies are needed to further verify the value of the radiomic model for small ccRCC, which is of great importance to urologists. For a radiomics study, our numbers were on the small side.

### Conclusion

The radiomic signature from multiparameter MRI can distinguish high-grade ccRCC from low-grade ccRCC with good performance. The radiomic model combining a radiomic signature and clinicoradiologic characteristics could improve the predictive performance of high-grade ccRCC, and thus can provide physicians noninvasively preoperative characterization of ccRCC.

### References

- Motzer RJ, Jonasch E, Agarwal N, et al. Kidney cancer, version 2.2017, NCCN clinical practice guidelines in oncology. *J Natl Compr Canc Netw* 2017;15:804-834.
- Escudier B, Porta C, Schmidinger M, et al. Renal cell carcinoma: ESMO clinical practice guidelines for diagnosis, treatment and follow-up. *Ann Oncol* 2016;27:v58-v68.
- Dagher J, Delahunt B, Rioux-Leclercq N, et al. Clear cell renal cell carcinoma: Validation of World Health Organization/International Society of Urological Pathology grading. *Histopathology* 2017;71:918-925.
- Moch H, Cubilla AL, Humphrey PA, Reuter VE, Ulbright TM. The 2016 WHO classification of tumours of the urinary system and male genital organs—Part a: Renal, penile, and testicular tumours. *Eur Urol* 2016;70:93-105.
- Leveridge MJ, Finelli A, Kachura JR, et al. Outcomes of small renal mass needle core biopsy, nondiagnostic percutaneous biopsy, and the role of repeat biopsy. *Eur Urol* 2011;60:578-584.
- Pedrosa I, Chou MT, Ngo L, et al. MR classification of renal masses with pathologic correlation. *Eur Radiol* 2008;18:365-375.
- Parada Villavicencio C, Mc Carthy RJ, Miller FH. Can diffusion-weighted magnetic resonance imaging of clear cell renal carcinoma predict low from high nuclear grade tumors. *Abdom Radiol* 2017;42:1241-1249.
- Rosenkrantz AB, Niver BE, Fitzgerald EF, Babb JS, Chandarana H, Melamed J. Utility of the apparent diffusion coefficient for distinguishing clear cell renal cell carcinoma of low and high nuclear grade. *AJR Am J Roentgenol* 2010;195:W344-W351.
- Cornelis F, Tricaud E, Lasserre AS, et al. Multiparametric magnetic resonance imaging for the differentiation of low and high grade clear cell renal carcinoma. *Eur Radiol* 2015;25:24-31.
- Dong D, Tang L, Li ZY, et al. Development and validation of an individualized nomogram to identify occult peritoneal metastasis in patients with advanced gastric cancer. *Ann Oncol* 2019;30:431-438.
- Peng H, Dong D, Fang MJ, et al. Prognostic value of deep learning PET/CT-based radiomics: Potential role for future individual induction chemotherapy in advanced nasopharyngeal carcinoma. *Clin Cancer Res* 2019;25:4271-4279.
- Song J, Shi J, Dong D, et al. A new approach to predict progression-free survival in stage IV EGFR-mutant NSCLC patients with EGFR-TKI therapy. *Clin Cancer Res* 2018;24:3583-3592.
- Zhang B, Tian J, Dong D, et al. Radiomics features of multiparametric MRI as novel prognostic factors in advanced nasopharyngeal carcinoma. *Clin Cancer Res* 2017;23:4259-4269.
- Dong D, Zhang F, Zhong LZ, et al. Development and validation of a novel MR imaging predictor of response to induction chemotherapy in locoregionally advanced nasopharyngeal cancer: A randomized controlled trial substudy (NCT01245959). *BMC Med* 2019;17:190.
- Liu Y, Zhang Y, Cheng R, et al. Radiomics analysis of apparent diffusion coefficient in cervical cancer: A preliminary study on histological grade evaluation. *J Magn Reson Imaging* 2019;49:280-290.
- Niu XK, Chen ZF, Chen L, Li J, Peng T, Li X. Clinical application of biparametric MRI texture analysis for detection and evaluation of high-grade prostate cancer in zone-specific regions. *AJR Am J Roentgenol* 2018;210:549-556.
- Peng H, Long F, Ding C. Feature selection based on mutual information: Criteria of max-dependency, max-relevance, and min-redundancy. *IEEE Trans Pattern Anal Mach Intell* 2005;27:1226-1238.
- Vallieres M, Zwanenburg A, Badic B, Cheze Le Rest C, Visvikis D, Hatt M. Responsible radiomics research for faster clinical translation. *J Nucl Med* 2018;59:189-193.
- Ma Z, Fang M, Huang Y, et al. CT-based radiomics signature for differentiating Borrmann type IV gastric cancer from primary gastric lymphoma. *Eur J Radiol* 2017;91:142-147.
- Wu Y, Kwon YS, Labib M, Foran DJ, Singer EA. Magnetic resonance imaging as a biomarker for renal cell carcinoma. *Dis Markers* 2015;2015:648495.
- Liu Z, Wang S, Dong D, et al. The applications of radiomics in precision diagnosis and treatment of oncology: Opportunities and challenges. *Theranostics* 2019;9:1303-1322.
- Shu J, Tang Y, Cui J, et al. Clear cell renal cell carcinoma: CT-based radiomics features for the prediction of Fuhrman grade. *Eur J Radiol* 2018;109:8-12.
- Bektas CT, Kocak B, Yardimci AH, et al. Clear cell renal cell carcinoma: Machine learning-based quantitative computed tomography texture analysis for prediction of Fuhrman nuclear grade. *Eur Radiol* 2019;29:1153-1163.
- Delahunt B, Eble JN, Egevad L, Samaratunga H. Grading of renal cell carcinoma. *Histopathology* 2019;74:4-17.

25. Sasaguri K, Takahashi N. CT and MR imaging for solid renal mass characterization. *Eur J Radiol* 2018;99:40-54.
26. Cui E, Li Z, Ma C, et al. Predicting the ISUP grade of clear cell renal cell carcinoma with– multiparametric MR and multiphase CT radiomics. *Eur Radiol* 2020;30:2912-2921.
27. Coy H, Young JR, Douek ML, et al. Association of qualitative and quantitative imaging features on multiphasic multidetector CT with tumor grade in clear cell renal cell carcinoma. *Abdom Radiol* 2019;44:180-189.
28. Wei J, Zhao J, Zhang X, et al. Analysis of dual energy spectral CT and pathological grading of clear cell renal cell carcinoma (ccRCC). *PLoS One* 2018;13:e0195699.
29. Rosenkrantz AB, Wehrli NE, Melamed J, Taneja SS, Shaikh MB. Renal masses measuring under 2 cm: Pathologic outcomes and associations with MRI features. *Eur J Radiol* 2014;83:1311-1316.
30. Marconi L, Dabestani S, Lam TB, et al. Systematic review and meta-analysis of diagnostic accuracy of percutaneous renal tumour biopsy. *Eur Urol* 2016;69:660-673.